Reduced plaque size and inflammation in the APP23 mouse model for Alzheimer's disease after chronic application of polymeric nanoparticles for CNS targeted zinc delivery

Antonietta Vilella[a*], Daniela Belletti[b*], Ann Katrin Sauer[c,d], Simone Hagmeyer[c,e], Tasnuva Sarowar[c,e], Martina Masoni[c,e], Natalia Stasiak[a], John J. E. Mulvihill[f], Barbara Ruozi[b], Flavio Forni[b], Maria Angela Vandelli[b], Giovanni Tosi[b*], Michele Zoli[a*], Andreas M. Grabrucker[d,g*#]

[a]Department of Biomedical, Metabolic and Neural Sciences, Center for Neuroscience and Neurotechnology, University of Modena and Reggio Emilia, 41125 Modena, Italy

[b]Department of Life Sciences, Center for Neuroscience and Neurotechnology, University of Modena and Reggio Emilia, 41125 Modena, Italy

[c]Institute for Anatomy and Cell Biology, Ulm University, 89081 Ulm, Germany

[d]Department of Biological Sciences, University of Limerick, V95PH61 Limerick, Ireland

[e]WG Molecular Analysis of Synaptopathies, Neurology Dept., Neurocenter of Ulm University, 89081 Ulm, Germany

[f]Bernal Institute & School of Engineering, University of Limerick, Ireland

[g]Bernal Institute, University of Limerick, Limerick, Ireland

** these authors contributed equally*

[#]Corresponding author

Prof. Dr. Andreas M. Grabrucker
Department of Biological Sciences, University of Limerick
Analog Devices Bld. AD1-018
Casteltroy,
V94 PH61 Limerick, Ireland
Tel.: +353 61 237756
Email: andreas.grabrucker@ul.ie

Short title: *Reduced plaque size and inflammation in Alzheimer's after zinc delivery*

Abstract

A local dyshomeostasis of zinc ions in the vicinity of amyloid aggregates has been proposed in Alzheimer's disease (AD) due to the sequestration of zinc in senile plaques. While an increase in zinc levels may promote the aggregation of amyloid beta (Aβ), increased brain zinc might also be beneficial rescuing some pathological alterations caused by local zinc deficiency. For example, increased Aβ degradation by metalloproteinases, and a reduction in inflammation can be hypothesized. In addition, zinc may allow a stabilization of the number of synapses in AD brains. Thus, to evaluate whether altering zinc-levels within the brain is a promising new target for the prevention and treatment of AD, we employed novel zinc loaded nanoparticles able to deliver zinc into the brain across the blood-brain barrier. We performed *in vivo* studies using wild type (WT) and APP23 mice to assess plaque load, inflammatory status and synapse loss. Furthermore, we performed behavioral analyses. After chronically injecting these nanoparticles for 14 days, our results show a significant reduction in plaque size and effects on the pro-inflammatory cytokines IL-6 and IL-18. On behavioral level we could not detect negative effects of increased brain zinc levels in APP23 mice and treatment with g7-NP-Zn normalized the observed hyperlocomotion of APP23 mice. Therefore, we conclude that a targeted increase in brain zinc levels may have beneficial effects in AD.

Keywords: blood brain barrier, Alzheimer, drug delivery, Nanoparticle, Zn^{2+}, amyloid

Introduction

A neuropathological hallmark of Alzheimer's disease (AD) is the formation of amyloid plaques [1]. The amyloid beta (Aβ) peptide is able to aggregate and generate fibrils that are deposited to form these plaques [2,3], which exhibit neurotoxicity via increase of oxidative stress and alteration in cellular processes [4].
Altered levels of trace metals are associated with pathological events in neurodegenerative diseases [5,6]. Specifically, zinc-deficiency causes alterations in brain function and cognition [7]. Zinc is highly concentrated in the Aβ plaques, for example shown in post mortem brain samples and also in AD transgenic mouse models [8].
Aβ plaques act as a metal sink causing zinc ions to reach abnormally high concentrations with depleted levels in the surrounding vicinity [8]. This zinc-ion sequestration by Aβ leads to decreased synapse density [9], and increased expression of pro-inflammatory cytokines. Therefore, local zinc deficiency may lead to activation of microglia and astrocytes resulting in cell death and neuroinflammation [10-12].
Zinc levels in the brain are tightly maintained [13] due to the blood-brain barrier (BBB) impermeability of the ion. Studies indicate that zinc traverses the plasma membranes on the luminal surface of the endothelial cells within the BBB [14-16]. As a hydrophilic and charged ion, transporters are therefore needed that restrict uptake. Although *in vitro* studies have shown that low levels of zinc induce protease-resistant aggregation of Aβ [11], Aβ degradation involves metalloproteinases, which need zinc ions for proper function [12]. It is thus necessary to understand the consequences of varying levels of zinc on the pathology of AD. However, few methods so far have been available to reach a fast and significant increase in brain zinc.

Previously, we examined the ability of zinc-loaded polylactide-co-glycolide (PLGA) nanoparticles (NPs), with a glycopeptide consisting of 7 amino acids (g7), to cross the BBB [17]. These modified NPs were shown to effectively transport therapeutic agents across the BBB [18], and demonstrated increased brain zinc levels post-injection [19]. Therefore, these NPs are a non-invasive, non-toxic and time-efficient method to selectively enrich brain zinc levels [19,20].
Here, we performed chronic application of zinc-loaded NPs in wild-type and APP23 mice. We evaluated the effect zinc-loaded NPs have on plaque load, inflammation and synapse stability, as well as plaque amount, plaque area, and zinc concentration. Further, behavioral analyses were performed to assess activity, anxiety and cognition of treated mice.

Material and Methods

Materials, chemicals and reagents
Poly(D,L-lactide-co-glycolide) (PLGA,RG503H, MW near to 11,000) was used as received from the manufacturer (Boehringer-Ingelheim, Ingelheim am Rhein, Germany). Gly-L-Phe-D-Thr-Gly-L-Phe-L-Leu-LSer(O-β-D-Glucose)-$CONH_2$ (g7) was prepared as described previously and conjugated with PLGA to obtain g7-PLGA [17,20-23]. The PLGA derivatization - yield was confirmed by NMR, from the relative peak area of the signals at 7.2–7.5 ppm, and of the multiplet at 1.80–1.60 ppm corresponding to the aromatic protons of the Phe and protons of the methyl groups of the polymer, respectively, and was found to be in the range of 30–40 μmol peptide/g of polymer. Zinpyr-1 was purchased from Sigma Aldrich and Santa Cruz. Primary antibodies were purchased from Merck Millipore ($Aβ_{1-42}$ and OC), and Synaptic Systems (Bassoon). Alexa Fluor conjugated secondary antibodies were from

Invitrogen. Secondary HRP conjugated antibodies were purchased from Dako. A MilliQ water system (18MΩ) (Millipore, Bedfrod, USA) provided distilled high-purity water. Unless otherwise indicated, all other chemicals were of analytical grade and obtained from Sigma-Aldrich (Milan, Italy).

Nanoparticles preparation and characterization

NPs were prepared as described in the literature [24] with some modifications in the preparation procedure. For the formulation of g7-NPs-Zn , $ZnSO_4$ (350 mg) was dissolved in distilled water (0.5 ml) and emulsified by sonication over an ice-bath using a probe sonicator (Misonix, MicrosonTM Ultrasonic Cell Disruptor XL, Opto-lab, Concordia, Mo, Italy) at 80 W output for 45 s with a polymeric solution in dichloro-methane (DCM, 2.5 ml), containing a mixture of PLGA 503 H and g7-PLGA (80:10 w/w). The resulting primary emulsion was added to distilled water (5 ml) containing 1% w/v polyvinyl alcohol (PVA, 15000 MW, Sigma- Aldrich) and sonicated for 45 s at 80 W amplitude over an ice-bath to form the double emulsion. Double emulsion was diluited with 3 ml of distilled water containing 1% w/v of PVA and stirred at room temperature (RT) (1,400 rpm) until the organic solvent was removed (at least 1 h) and finally purified by high-speed refrigerated centrifugation (Beckman J21) at 14,000 rpm for 10 min.

To obtain unloaded NPs (g7-NPs) used as control, we applied the same procedure without adding $ZnSO_4$ to the hydrophilic phase. All batches of the NPs were characterized in terms of their surface, chemico-physical, and morphological properties. In particular, for surface properties (size and surface charge), NPs suspended in distilled water were analyzed by photon correlation spectroscopy (PCS) and laser Doppler anemometry using a Zetasizer Nano ZS (Malvern, UK; Laser 4 mW He–Ne, 633 nm, Laser attenuator Automatic, transmission 100% to 0.0003%, Detector Avalanche photodiode, Q.E. > 50% at 633 nm, T = 25°C). The results were normalized with respect to a polystyrene standard solution.

To evaluate the shape and morphology of NPs, a scanning electron microscope (SEM) (XL-40; Philips, Eindhoven, Netherlands) operating at 8 kV was used. NPs were re-suspended in distilled water after washing at least thrice with water. A drop of the suspension was placed onto the SEM sample holder and dried under vacuum (10–2 mmHg). The dried samples were coated with gold palladium with a thickness of 10 nm (Emitech K550 Super Coated; Emitech Ltd, Ashford, Kent, UK) under argon atmosphere to increase electrical conductivity. The NPs were then processed for the evaluation of their morphology and shape by analyzing images at different magnifications (13,000× to 16,000×).

Evaluation of zinc content

To determine the Zn^{2+} content, an exact amount of NPs (10 mg) loaded with $ZnSO_4$ (g7-NPs-Zn) were dissolved in DCM (1 ml), and MilliQ water (5 ml) was added to the organic solution. The organic solvent was removed by stirring at RT for at least 3 h, and finally the aqueous solution was filtered through a syringe filter (cellulose acetate, 0.45 μm) to remove water-insoluble polymer. The final volume of the aqueous solution was adjusted to 50 ml with distilled water. This final aqueous solution was analyzed using atomic absorption spectrophotometry.

Evaluation of zinc - release from NPs

The release of Zn^{2+} from loaded NPs samples was assessed by means of dialysis method as reported before [19]. Briefly, a weighted sample of NPs (1 mg) was suspended in distilled water and placed in a dialysis membrane (Spectra/Por 7 MWCO:10000) of 5 cm length. The membrane was maintained under stirring in a receiving environment (distilled water or

phosphate buffer pH 7.4) at 37°C. At established time points, samples were retrieved for complexometric analysis. All data were obtained in triplicate for each NPs sample analyzed.

Evaluation of PVA residual

As residual PVA associated with NPs could affect their physical properties and cellular uptake, the amount of PVA was determined by a colorimetric method based on the formation of a colored complex between two adjacent hydroxyl groups of PVA and an iodine molecule. Briefly, freeze-dried samples (5 mg) were solubilized in DCM (1 ml). Then, distilled water (2 ml) was added and the organic solvent was evaporated at RT under stirring (for 2 h). The suspension was filtered (cellulose nitrate filter, porosity 0.45 μm, Sartorius, Florence, Italy) to remove the polymeric residue, and the aqueous solution (1 ml) was treated with 0.5 M NaOH (2 ml) for 15 min at 60°C. The solution was neutralized with 1 N HCl (900 μl) and the volume adjusted to 5 ml with distilled water. Then, a solution of 0.65 M boric acid (3 ml), I2/KI (0.05 M/0.15 M, 0.5 ml), and distilled water (1.5 ml) was added. PVA concentration was determined by measuring the absorbance at 690 nm after 15 min of incubation at RT and compared to a standard plot of PVA prepared under the same experimental conditions.

Animals

18 month-old mice, *Mus musculus,* strain C57BL/6 and APP23 (maintained on the same background) of both genders were used. The animals were housed in plastic cages with stainless steel mesh lids under the standard laboratory condition with temperature 22-24°C, food and water available *ad libitum*, humidity 55% +/- 10% and 12/12 h light/dark cycle (lights on at 7 AM). The weight of the animals was 25 - 30g. $APP23^{+/-}$ and wild type received two daily i.p. injection of exact amounts of NPs or saline, one during the morning and the second during the evening, for 14 consecutive days. All animal experiments were performed in compliance with the guidelines for the welfare of experimental animals issued by the Federal Government and approved by the local ethics committee of the University of Modena and Reggio Emilia. Mice were divided into groups (n=7 for WT_{Saline}, APP_{Saline}, $WT_{g7\text{-}NPs}$, n=6 for $APP_{g7\text{-}NPs}$, n=18 for $WT_{g7\text{-}NPs\text{-}Zn}$, $WT_{g7\text{-}NPs\text{-}Zn}$) and males and females analysed. As no gender specific effects were detected, data for both genders was pooled.

Behavioral analysis

In this study, three behavioral tests were performed in the following order: Open field (OF), 7 d after first treatment, elevated plus maze (EPM) on day 10, fear conditioning (FC) on days 13-14. All tests were performed 3 hours after the first daily injection of NPs or saline.

OF test: the OF test was performed in an arena of 50 x 50 cm with dark walls and floor and virtually divided by software in a peripheral area located 10 cm from the wall and a 30x30 cm central area and further subdivided into virtual squares. The animal was placed at the center of the arena. Behavior was recorded for 10 min using a camera positioned above the OF and connected to an ANY-MAZE video tracking system. For behavioral analysis, the entries from peripheral to central area and the transitions between virtual squares were evaluated. After each test, the arena was cleaned with 70% ethanol to avoid the presence of olfactory stimuli related to the previous animal.

EPM test: the EPM was performed in an apparatus with two open arms and two closed arms, lifted 70 cm from the floor. The test started by placing the animal in the center of the maze with the head turned towards the closed arm. The animal was allowed to freely explore the apparatus for 5 min and the performance was recorded by the ANY-MAZE video tracking system. The number of entries and the time spent in the open and closed arms were considered. After each test, the apparatus was cleaned with 70% ethanol to avoid the presence of olfactory stimuli related to the previous tested animal.

FC test: in this study, FC was performed as previously described [25,26]. Briefly, mice were transferred into an acoustically isolated (23 x 22 x 24 cm) conditioning chamber with walls and ceiling in grey Plexiglas and a floor consisting of stainless steel bars connected with a device able to produce an electrical shock. After a period of initial acclimatization of 2 min, the animal was subjected to 3 foot shocks (0.5 mA, 2 s) separated by 2 min of rest and the mice were removed from the chamber 30 s after the last shock. Approximately 24 h after conditioning, mice were tested for contextual conditioning. Mice were placed in the conditioning chamber for 5 min and freezing behavior was scored. Freezing was scored using a time sampling procedure in which every 10 s a determination was made whether or not mice showed the freezing behavior. Freezing was defined as the absence of all movement except for respiration for a minimum of 1 s. After each test, the chambers were cleaned with 70% ethanol to avoid the presence of olfactory stimuli related to the previous animal.

Histochemistry

Brain sections (14 µm thickness) were prepared from frozen using a cryostat (Leica CM 3050S) with the knife set at -23°C. Three sections of the brain of the same animal were collected on one microscope slide. For staining, the slices were fixed with PFA/4% Sucrose for 20 min at RT. After washing 3x 5 min with 1x PBS, incubation with Triton 0.2% in 1x PBS for 1 h at RT was followed by incubation with Triton 0.05% for 10 min at RT. Subsequently, the slides were covered with Blocking Solution (BS: 10% FCS in PBS) for 2 h at RT. The primary antibody was diluted in BS and applied over-night at 4°C. The next day, incubation for 10 min with Triton 0.05% at RT was followed by incubation with the secondary antibody coupled to Alexa488, diluted 1:500 in BS, at 37°C for 2 h. After a 3x 15 min washing-step with Triton 0.05% and 1x 5 min with 1x PBS, cell nuclei were counterstained with DAPI and after the last washing step with 1x PBS for 5 min, cover slips were mounted using Vecta Mount (Vector Laboratories).

Zinpyr-1 staining was performed at a final concentration of 10 □M and incubation time of 1 h at RT. Sections were counterstained with DAPI and mounted with Vecta Mount (Vector Laboratories).

For Thioflavin S staining, sections were thawed for 20 minutes at RT. After fixation with 4% PFA for 20 minutes sections were washed with 80%, 70% and 50% EtOH for 1 min each and stained with Thioflavin S (0.1% dissolved in 50% EtOH) for 25 min. Afterwards, they were washed with 50%, 70% and 80 % EtOH for 1 minute each. After counterstaining with DAPI, sections were washed with ddH_2O and mounted with Vectamount.

Protein biochemistry

Dot blot analysis was performed using a PVDF membrane wetted with 100% methanol. The membrane was incubated with transfer buffer for 2-3 min and protein lysate spotted on and incubated overnight. Subsequently, the membrane was washed 2x with TBST buffer 0.05% and blocked with TBS containing 5% non-fat dry milk for 30 min at RT on a shaker, followed by application of the primary antibody for 2 h at RT on a shaker. After washing 4 times for 5 min each with TBST buffer 5%, incubation with secondary HRP antibodies was performed for 1 h at RT. Immunoreactivity was visualized using the SuperSignal detection system (Pierce, Upland, USA) and blots imaged using a MicroChemi Imaging System from Biostep. 3 µg protein were loaded onto membranes and loading was controlled using Ponceau S staining. Immunoreactive signals were normalized to Ponceau S signals performing quantification of signals with ImageJ.

Quantitative Real-time PCR

Isolation of total RNA from mouse brains per group was performed using the AllPrep

RNA/Protein kit (Qiagen) as described by the manufacturer. The protocol was followed until step 6. Then, the APL buffer (Qiagen) was added and the Sonicator SonoPlus used 3x for 10 s each. The homogenate was loaded on a QIAshredder spin column (Quiagen) and centrifuged at 10000 rpm for 3 min. The flow-through was collected and the RNA/Protein isolation continued at step 10 of the protocol. mRNA was obtained and the concentration and purity measured with a NanoDrop 2000 UV-Vis Spectrophotometer.
Quantitative RT-PCR amplification was carried out in a one-step, single-tube format using the QuantiFast SYBR Green RT-PCR kit and a Rotor-Gene-Q real-time PCR machine (model 2-Plex HRM) (Qiagen). The qRT-PCR was assayed in 0.1 ml strip tubes with a total volume of 20 µl reaction mixture containing 1 µl of undiluted (normalization: Dilution to the lowest concentration 758.6 ng/µl) RNA, 2 µl of QuantiTect Primer Assay oligonucleotides, 10 µl of 2x QuantiFast SYBR Green RT-PCR Master Mix supplemented with ROX (5- carboxy-X-rhodamine) dye, 6.8 µl of RNase-free water and 0.2 µl of QuantiFast RT Mix. The following primer were used: Il-6 (Mm_Il6_1_SG; #QT00098875), Il-10 (Mm_Il10_1_SG; #QT00106169), Il-18 (Mm_Il18_1_SG; #QT00171129), Tnf (Mm_Tnf_1_SG; #QT00104006), Hmbs (Mm_Hmbs_1_SG; #QT00494130). Amplification conditions were as follows: 10 min at 55°C, 5 min at 95°C, followed by 40 cycles of PCR for 5 s at 95°C for denaturation, 10 s at 60°C for annealing and elongation (one-step). The SYBR Green I reporter dye signal was measured against the internal passive reference dye (ROX) to normalize non-PCR-related fluctuations. Resulting data were analyzed utilizing the hydroxymethylbilane synthase (Hmbs) gene as an internal standard. Cycle threshold (ct) values were calculated by the Rotor-Gene-Q Software (version 2.0.2). All qRT-PCR reactions were run in triplicates and mean ct values for each reaction were taken into account for data analysis. A melting curve was obtained for the amplicon products to determine their melting temperatures.

Measurement of Zn^{2+} concentrations
The zinc-concentration of brain tissue was measured by atomic absorption spectrometry (AAS) at the Department of Clinical Chemistry (ZE klinische Chemie) of the University Hospital Ulm. Samples for ASS were prepared by homogenizing tissue in Buffer A (320 mM sucrose, 5 mM HEPES pH 7.4). Proteinase K was added to the crude homogenate and incubated at 37°C for 1 h. The cell debris and blood cells were removed by centrifugation at 3,200 rpm for 10 min at RT. The supernatant was collected and analyzed by AAS.

Statistics
Fluorescence images were obtained using an upright Axioscope microscope equipped with a Zeiss CCD camera (16 bits; 1280x1024 ppi) using Axiovision software (Zeiss) (Zinpyr1 staining) and a LSM 710 confocal microscope from Zeiss with ZEN 2011 software. Analyses were performed with ImageJ 1.51a. For the analysis of plaque load, three images of the cortex for each sample were obtained in a five-fold magnification. The number and the area of the plaques were measured and the number of plaques per square pixel was calculated.
Statistical analysis was performed with SPSS version 20. Data are shown as mean ± SEM. Groups were compared using two-way ANOVA and post-hoc Bonferroni analysis was performed. The level of significance was set at 0.05 (<0.05*; <0.01**; <0.001***).
qRT PCR quantification – Relative quantification is based on internal reference genes to determine virtual mRNA levels of target genes. Cycle threshold (ct) values were calculated by the Rotor-Gene Q Software (version 2.0.2). Ct values were transformed into virtual mRNA levels according to the formula: virtual mRNA level = $10 * ((ct_{(target)} - ct_{(standart)}) /$ slope of standard curve).

Results and Discussion

Currently, there is no cure for AD. However, since the formation of plaques made of Aβ peptide is at the center of AD pathology, one interesting strategy of treatment could be the reduction of the number of these aggregates and with this the normalization of processes affected by plaque formation. One of these processes is zinc homeostasis. The sequestration of zinc within Aβ plaques decreases the availability of zinc affecting its physiological functions in the brain. For this reason, models predict that an increase of bioavailable zinc in the brain could overcome the losses caused by zinc binding to Aβ. However, as the sequestration of zinc in plaques might not induce a systemic zinc deficiency and zinc is rather mislocalized than decreased in general, an important obstacle to zinc enrichment is represented by the BBB and its tight selectivity. However, new nanotechnological drug delivery systems are available to allow zinc passage through the BBB [19].

Here, we studied PLGA-based NPs loaded with zinc and labeled with a glycopeptide, consisting of 7 amino acids for BBB crossing. Polymer-based NPs are the most widely used nanotechnology for drug delivery because these compounds are normally biodegradable, they do not accumulate in the body, and they are relatively risk-free [27]. Currently, some few polymers guarantee the safety of nanocarriers, among them PLGA, which is therefore one of the most promising polymers for the preparation of NPs [28].

Nanoparticle characterization and mouse model

NPs (g7-NPs and g7-NPs-Zn) were characterized in their chemical–physical properties (Figure 1A-C). All samples, independent of loading, were featured by the hydrodynamic diameters (Z-Average) around 200-220 nm and relatively narrow size distributions (polydispersivity, PDI<0.15), favorable for a systemic administration. Surface charge expressed as Z-pot was negative accordingly to the exposure of carboxylic group of the polymer.

The loading capacity (L.C.) was approximately 7% corresponding to 72 μg of Zn/mg of g7-NPs-Zn. As expected, Zn release from NPs, tested over time in different pH solutions, resulted always in extremely rapid release completed over 2 hours (Fig. 1C) due to the chemical MW and properties of Zn, which is very difficult to keep entrapped into the polymeric matrix. However, previous studies show that NPs rapidly enter the brain [17,21] even within 5-20 min, with peak accumulation in the CNS around 60-120 min after application. As we have also shown that g7-NPs-Zn significantly increase brain Zn levels 3 hours after injection in contrast to injection of Zn solution [19], we conclude that within this timeframe, g7-NPs are able to transfer Zn across the BBB and produce a very quick release within the CNS compartment.

The animals used in this work were 18 month-old heterozygous $APP23^{+/-}$ transgenic mice (APP23) and wild-type (WT) $APP23^{-/-}$. The APP23 mouse model is a well-described model for AD [29] that develops amyloid plaques and amyloid pathology as seen in human AD with neurodegeneration [30]. After injections, animals treated with g7-NPs-Zn received a total of 392 μg Zn. Injection of Zn solution and NPs-Zn in comparision to g7-NPs was performed before [19]. Zn solution did not significantly increase brain Zn levels, and NPs-Zn lead to slightly lesser increase compared to g7-NPs-Zn. Therefore g7-NPs-Zn were chosen here. As reported previously [19], we observed sleepiness directly after injection of Zn-g7-NPs lasting not more than 1 hour. 3 hours after administration of NPs-Zn, we found a significant increase of Zn levels in brain (assessed by ICP-MS) of about 20% with respect to injection of saline solution [19].

A second measurement of the lysate of the right hemisphere of mice after chronic administration and behavioral experiments using AAS did not show a significant increase in zinc concentration after treatment with g7-NP-Zn (Fig. S1A). It is likely that after administration, zinc is rapidly released from NPs but compensatory mechanism in the brain might reduce zinc levels back to normal some time after the last administration. Given that the analysis was performed after the last dose of g7-NP-Zn, brain zinc levels were already normalized. Thus, in the following experiments, we investigated whether lasting changes related to the AD pathology occurred. WT and APP23 mice were treated with saline solution as control condition, with g7-NPs to observe any effects of the NPs, and with g7-NP-Zn to study the action of zinc. After behavioral experiments, we evaluated inflammation, synapse density and the effects of zinc on Aβ plaques.

Reduced plaque size in animals treated with zinc-loaded nanoparticles
Amyloid-related degenerative diseases are associated with the accumulation of misfolded proteins as amyloid fibrils in tissue. To visualize the plaques in the cortex of APP23 mice, brain sections of the right hemisphere were stained using an anti-Aβ antibody. The mean plaque area and the number of plaques per square pixel in frontal cortex were measured and quantified (Fig. 2A-C). As expected, none of the WT animals showed plaques. In the APP23 animals, between the groups treated with saline and g7-NP-Zn, and g7-NP and g7-NP-Zn, a significant difference was detected. The mean plaque area was significantly decreased after treatment with g7-NP-Zn (Fig. 2A). The number of plaques per area, however, was unaffected (Fig. 2C). We repeated the experiments using Thioflavin as alternative method to visualize plaques (Fig. 2D,E). We could confirm a significant reduction in plaque area in APP23 mice treated with g7-NP-Zn compared to saline and g7-NP-treated mice. The number of plaques per area in the same group was not significantly ($p = 0.13$) reduced (Fig. 2D).

Aβ accumulates in different types of insoluble plaque deposits, intracellular Aβ and soluble oligomers. Conformation-dependent antibodies specifically recognize distinct assembly states of amyloids, including prefibrillar oligomers and fibrils. The OC antibody is able to recognize fibrillary oligomers that are immunologically distinct from prefibrillar oligomers recognized by the anti- Aβ antibody used before [31]. To verify the results obtained, we performed protein biochemistry using protein lysate from cortex of APP23 and WT mice. Dot Blot analysis using the OC antibody did not shows any significant change in fibrillary oligomers in APP23 mice injected with g7-NP-Zn (Fig. 2F) compared to Saline and g7-NP injected mice. The zinc content of plaques was not significantly altered. Amyloid plaques were visualized with Zinpyr-1 [9] and no change in Zinpyr-1 signal intensity was detected. Measuring plaque area and number, we obtained similar results as those seen using anti- Aβ antibody staining showing a significant decrease in plaque area, but not number of plaques, between saline injected APP23 controls and APP23 mice treated with g7-NP-Zn (Fig. 3A-B).
The detected alterations in plaque size were less pronounced in the hippocampus (Fig. S1B). Using Thioflavin to visualize plaques we could not detect any significant reduction in plaque area or number per area in APP23 mice treated with g7-NP-Zn in the hippocampus (Fig. S1B).

A reduction of plaque area may be caused by both disassembly / degradation of Aβ aggregates and slowed down aggregation. The duration of treatment however favours a model of degradation. The absence of significant changes in the number of plaques per square pixel may be due to the fact that the treatment started at an age when plaques had already formed in APP23 mice [32]. Therefore, it might be worth investigating the effect of g7-NP-Zn on the

prevention of plaque formation in future studies. Additionally, it might be possible that treatment for a longer period of time or with different concentrations of NPs will also affect the number of plaques present in the brain. Further, we did not detect a decrease in plaque size in the hippocampus. As zinc levels reached a high concentration in the hippocampus under physiological conditions, additional delivery of zinc using NP may have a less pronounced effect there. In addition, NP distribution and alternative expression of zinc dependent proteins such as matrix metalloproteinases may account for differences across brain regions.

Zinc levels correlate with levels of IL-6 and IL-18 and zinc loaded nanoparticles alter inflammatory markers in APP23 animals

Biochemical and neuropathological studies of brains from individuals with AD provide evidence for an activation of inflammatory pathways [33]. Genetic studies using mice confirmed that inflammatory cytokines have potent effects on amyloidosis, neurodegeneration, and cognition. These proteins can strongly activate glial cells and induce neuroinflammation. Therefore, we evaluated the action of increased levels of zinc in the brains of APP23 mice on inflammation. For this reason, the expression levels of IL-6 and IL-18, pro-inflammatory cytokines, IL-10, an anti-inflammatory cytokine, and TNF1, an inflammatory cytokine that mediates local and systemic inflammation, were quantified in mouse brain tissue (Fig. 4).

As expected, APP23 mice treated with saline solution or empty g7-NPs showed higher levels of pro-inflammatory cytokines compared with the corresponding group of WT mice. Despite large individual differences, our results show increased levels of IL-6 in APP23 mice compared to WT mice (Fig. 4A). The levels of IL-6 significantly decreased in APP23 animals treated with NPs loaded with zinc compared to the mice injected with empty NPs (Fig. 3A). However, the absence of a clear inflammatory phenotype in APP23 mice interfered with the subsequent assessment of beneficial effects of zinc delivery regarding neuro-inflammation. Treatment with g7-NPs-Zn had no significant effect on WT animals.

IL-18 is a pro-inflammatory cytokine, able to induce the amyloidogenic processing of APP [34]. Furthermore, an increased level of total- RNA and protein of IL-18 was reported in AD patients [35]. For IL-18, similar levels of IL-18 were found in APP23 mice compared to WT mice (Fig. 4B), but a significant decrease of this cytokine was detected in APP23 mice injected with g7-NP-Zn compared to APP saline injected animals and APP23 mice injected with empty NPs (Fig. 4B). Again, the treatment with g7-NP-Zn had no effect on WT mice.

TNF is another important pro-inflammatory cytokine upregulated in AD patients [36]. Here, we measured the mRNA level of TNF-1, but could not observe significant differences between APP and WT mice treated with loaded and unloaded NPs, and no correlation with brain-zinc levels (Fig. 4C). None of the differences in TNF-1 measured between groups and treatment conditions was significant possibly due to high inter-individual differences of APP23 mice.

IL-10 is an anti-inflammatory cytokine able to limit inflammation through different mechanisms: reducing the synthesis of pro-inflammatory cytokines, such as IL- 1 and TNF-α, suppressing cytokine receptor expression, and inhibiting receptor activation in the brain. The level of IL-10 was found similar in saline-injected APP23 mice compared to WT mice and higher in g7-NP injected APP23 mice compared to WT g7-NP-injected mice ($p = 0.015$). The groups treated with g7-NP-Zn, both in WT ($p = 0.0074$) and APP23 ($p = 0.55$) mice showed

an increase in anti-inflammatory IL-10 (Fig. 4D). Thus, an increase in brain zinc seems to alter IL-10 levels independent from the presence of an AD pathology. Taken together, these results might suggest that g7-NP-Zn are able to decrease pro-inflammatory responses and increase anti-inflammatory cytokines, counteracting inflammatory processes. However, more research is needed in future.

Given the variability of individuals within the analyzed groups, we performed a correlation analysis of the measured parameters based on measured values for each individual. We could not detect a significant correlation between brain zinc concentration and plaque load in APP23 mice or a significant correlation between plaque load and levels of IL-6, IL-18, TNF-1, and IL-10. However, we detected a significant correlation between brain zinc levels and the expression of IL-6 and IL-18, both cytokines that showed significant response to g7-NP-Zn treatment (Fig. 4E,F). This correlation was particularly pronounced in the group treated with g7-NP-Zn. This correlation was absent in WT mice, and no correlation between zinc levels and IL-10 or TNF-1 was detected. Our data suggest that the higher the zinc level in the brain of a mouse, the lower may be the expression of the pro-inflammatory cytokines. In particular, the correlation is visible in APP23 mice, possibly due to the presence of neuro-inflammation which, however, was hard to detect on population level. However, we have analysed total zinc levels rather than chelatable zinc, which may mask some correlations.

Zinc levels correlate with synapse density in APP23 mice

Synaptic plasticity is important for memory and learning, and persistent disruption of plasticity or loss of synapses may explain the cognitive decline in later phases of AD. A loss of synaptic contacts in AD appears to be an early event in AD pathogenesis [37]. Quantification using electron microscopy or immunohistochemical staining for synaptic markers has documented significant decreases of synaptic density in AD patients [38,39]. Also, it has been shown that APP23 mice display dendrite degeneration and synapse loss [40].

Thus, in a further set of experiments, we measured and quantified the number of synapses after treatment, especially since zinc plays an important role in synaptic plasticity [41], and it was shown that zinc sequestration by Aβ causes a SHANK3-dependent loss of synapses that could be rescued by zinc supplementation *in vitro* [9]. Thus, brain sections were stained for Bassoon, a protein localized at the pre-synaptic nerve terminal and involved in the structural and functional organization of the pre-synaptic active zone of inhibitory and excitatory synapses (Fig. 5A,B). No significant change in synapse density was detected between the different treatment groups (Fig. 5A). We again performed a correlation analysis of the measured parameters based on measured values for each individual. The concentration of zinc showed a significant correlation with the number of synapses per area selectively in APP23 mice across all groups (Fig. 5C). However, these results are hard to interpret as there is an absence of a clear phenotype in the APP23 mice when treated with g7-NP-Zn.

Several mechanisms might be responsible for beneficial effects of increased zinc levels regarding synapse density. For example, it was shown *in vitro* that the presence of Aβ acts as a sink for zinc ions, depleting zinc-dependent synaptic scaffold proteins of the SHANK family of zinc that is needed for PSD platform formation [42,9,43]. In addition, increased levels of zinc may lead to increased levels of brain-derived neurotrophic factor (BDNF) [44], which in turn promotes synapse formation [45,46]. Further, a reduction of oxidative stress by rescuing local zinc deficiency may have beneficial effects on cell survival and ultimately synapse density [47]. Interestingly, in APP23 mice but not in WT mice, we found a clear correlation between the brain-zinc levels of an individual and the number of synapses in

cortex brain tissue. This was found across all treatment groups. Therefore, while the limited number of animals studied possibly prevented the demonstration of the expected loss of synapses in saline-treated APP23 mice in present experiments, our data indicate that, irrespective of zinc delivered by zinc-loaded NPs, differences in brain zinc concentration may have influence on synapse density in aged APP23 mice, and point to the therapeutic importance of pursuing brain zinc supplementation in AD.

Reduced hyperlocomotion in APP23 mice treated with g7-NP-Zn

Cognitive impairment is the main clinical feature of AD. Other common behavioral symptoms include increased anxiety, depression, a decrease of initiative and interest, and disinhibition [48]. In addition, locomotor deficits may occur. Hyperlocomotion associated with behavioral disinhibition has been reported in tg2576 mice, a mouse model for AD [49]. To evaluate possible effects of treatment with g7-NP-Zn at behavioral level, we performed behavioral tests using WT and APP23 mice after chronic treatment with saline, g7-NP and g7-NP-Zn.

First, to evaluate whether alterations in locomotor activity are present, an OF test was performed. As a measure of locomotor activity we considered the total number of transitions between the virtual squares of the OF (Fig. 6A). Two-way ANOVA showed a significant increase in locomotion in APP23 mice compared to WT mice. Post-hoc comparisons showed that a significant difference between genotypes was present in saline and g7-NP treated mice, but treatment with g7-NP-Zn normalized the observed hyperlocomotion of APP23 mice (Fig. 6A). We also considered a second parameter of OF test, i.e., the number of entries from external to internal area (Fig. 6B). Two-way ANOVA showed a significant increase in entries towards internal area in APP23 mice with respect to WT mice that was independent from treatments.

Secondly, in the EPM test, a test performed in an apparatus consisting of two open and two closed arms, no significant genotype-related change in anxiety like behavior (open arm entries/total entries) was found in APP23 mice compared to WT mice (Fig. 6C). Treatment with g7-NP or g7-NP-Zn showed no significant effect on anxiety like behavior (Fig. 6C). Additionally, no significant genotype-related changes in contextual FC test, one of the most used models for studying associative memory depending upon hippocampal function [50] were observed (Fig. 6D). Treatment with g7-NP or g7-NP-Zn showed no significant effect on associative memory (Fig. 6D).

The limited effects of g7-NP-Zn treatment in present behavioral tests was mostly due to the absence of significant differences between WT and APP23 mice in general. To ensure that APP23 mice had a full pathology (inflammation and plaques), we used relatively old mice (18 month-old). However, on behavioral level, WT mice may also suffer from impairments at this age, and/or plaque-related memory deficits derived from hippocampal dysfunctions may not be very pronounced at this age in APP23 mice. In addition, plaques were more concentrated in neocortical regions and the tests performed in this study are not well suited to assess cortical deficits. Thus, behavioral effects of treatment may have been poorly visible due to the absence of a clear phenotypic difference in APP23 mice in the tests performed. However, we can conclude that the treatment with g7-Zn-NP did not result in severe side effects, and did not negatively affect parameters such as locomotion or anxiety, irrespective of the genotype of mice. Future studies with long-term treatment and treatment starting before plaque formation begins might reveal more dramatic effects.

Conclusions

WT and APP23 mice were treated with g7-NP-Zn to study the action of increased brain zinc-levels on AD pathology. Taken together, application of g7-Zn-NPs, a non-invasive way to increase brain zinc levels in a matter of hours, in a mouse model for AD showed promising effects regarding a potential to decrease Aβ aggregation, stabilize synapses and decrease inflammation. A significant decrease in the mean plaque area was detected after treatment with g7-NP-Zn in APP23 mice. However, more research is necessary regarding time-point of application, duration, and concentration of NPs to find the most beneficial treatment strategy. Nevertheless, the study shows that increased zinc levels in the brain do not increase AD pathology in APP23 mice and mice did not show obvious side effects of chronic application of g7-Zn-NPs.

The finding that increasing zinc levels in the brain may be beneficial for AD might seem counterintuitive on first sight given the reported positive effects of zinc chelators such as Clioquinol and PBT2 on AD pathology. Clioquinol was reported to decrease plaque load as well [51]. However, our findings are in line with these results as Clioquinol has an affinity that allows it to bind to free zinc or weakly bound zinc [52], but it was shown to re-distribute this zinc for example to proteins in neurons [53] with higher affinity for the ion, or metalloproteases [54] that may participate in the degradation of Aβ aggregates. In our approach, we do not provide zinc to effector proteins by chelation of zinc from endogenous sources. Instead we delivered this zinc by NPs. This may have the advantage that the pool of endogenous chelatable zinc such as zinc in synaptic vesicles and zinc bound to proteins other than Aβ may not be affected. However, the downstream effectors mediating Aβ degradation after re-distribution or addition of zinc may be similar, underlining that targeting biometal homeostasis is a promising approach in AD.

Competing interests

The authors declare that they have no competing interests.

Acknowledgments

SH is a member of the international PhD program in molecular medicine of Ulm University and funded by Evangelisches Studienwerk Villigst e.V.. TS is supported under the Postgraduate Scholarships Act of the Land of Baden-Wuerttemberg (LGFG). The research was partially funded by MIUR grant (PRIN 2010-2011 - protocollo: 2010H834LS_003) and by FARUNIMORE 2014 (Tosi PI) and FARUNIMORE 2014 grant (Vandelli PI). The authors would like to acknowledge networking support by the COST Action TD1304.

References

[1] A. Burns, E.J. Byrne, K. Maurer, Alzheimer's disease. Lancet 360(9327) (2002) 163-165.

[2] H. Zhang, Q. Ma, Y.W. Zhang, H. Xu, Proteolytic processing of Alzheimer's β-amyloid precursor protein. J Neurochem 120 Suppl 1 (2012) 9-21.

[3] W.L. Klein, Abeta toxicity in Alzheimer's disease: globular oligomers (ADDLs) as new vaccine and drug targets. Neurochem Int 41(5) (2002) 345-352.

[4] V.H. Finder, R. Glockshuber, Amyloid-beta aggregation. Neurodegener Dis 4(1) (2007) 13-27.

[5] A.M. Grabrucker, Zinc in the developing brain, in: V.H. Moran, N. Lowe (Eds): Nutrition and the developing brain. CRC Press, (2016) pp.143-168.

[6] S. Grabrucker, A.M. Grabrucker, Chapter 9: Zinc and autism, in A. White (Ed): Biometals in Neurodegenerative Diseases: Mechanisms and Therapeutics. Elsevier, 2017 pp.153-173.

[7] R.I. Henkin, B.M. Patten, P.K. Re, D.A. Bronzert, A syndrome of acute zinc loss. Cerebellar dysfunction, mental changes, anorexia, and taste and smell dysfunction. Arch Neurol 32(11) (1975) 745-751.

[8] C.Y. Wang, T. Wang, W. Zheng, B.L. Zhao, G. Danscher, Y.H. Chen, Z.Y. Wang, Zinc overload enhances APP cleavage and Aβ deposition in the Alzheimer mouse brain. PLoS One 5(12) (2010) e15349.

[9] A.M. Grabrucker, M.J. Schmeisser, P.T. Udvardi, M. Arons, M. Schoen, N.S. Woodling, K.I. Andreasson, P.R. Hof, J.D. Buxbaum, C.C. Garner, T.M. Boeckers, Amyloid beta protein-induced zinc sequestration leads to synaptic loss via dysregulation of the ProSAP2/Shank3 scaffold. Mol Neurodegener (2011) 6:65.

[10] A.S. Prasad, Discovery of human zinc deficiency: its impact on human health and disease. Adv Nutr 4(2) (2013) 176-190.

[11] A.I. Bush, W.H. Pettingell, G. Multhaup, M. d Paradis, J.P. Vonsattel, J.F. Gusella, K. Beyreuther, C.L. Masters, R.E. Tanzi, Rapid induction of Alzheimer A beta amyloid formation by zinc. Science 265(5177) (1994) 1464-1467.

[12] C. Tallant, A. Marrero, F.X. Gomis-Rüth, Matrix metalloproteinases: fold and function of their catalytic domains. Biochim Biophys Acta 1803(1) (2010) 20-28.

[13] B. Lönnerdal, Dietary factors influencing zinc absorption. J Nutr 130 (5S Suppl) (2000) 1378-1383.

[14] S. Buxani-Rice, F. Ueda, M.W. Bradbury, Transport of zinc-65 at the blood-brain barrier during short cerebrovascular perfusion in the rat: its enhancement by histidine. J Neurochem. 62(2) (1994) 665-672.

[15] P.A. Franklin, R.G. Pullen, G.H. Hall, Blood-brain exchange routes and distribution of 65Zn in rat brain. Neurochem Res 17(8) (1992) 767-771.

[16] A. Takeda, Movement of zinc and its functional significance in the brain. Brain Res Brain Res Rev 34(3) (2000) 137-148.

[17] G. Tosi, R.A. Fano, L. Bondioli, L. Badiali, R. Benassi, F. Rivasi, B. Ruozi, F. Forni, M.A. Vandelli, Investigation on mechanisms of glycopeptide nanoparticles for drug delivery across the blood-brain barrier. Nanomedicine (Lond) 6(3) (2011) 423-436.

[18] R. Chhabra, G. Tosi, A.M. Grabrucker, Emerging Use of Nanotechnology in the Treatment of Neurological Disorders. Curr Pharm Des 21(22) (2015) 3111-3130.

[19] R. Chhabra, B. Ruozi, A. Vilella, D. Belletti, K. Mangus, S. Pfaender, T. Sarowar, T.M. Boeckers, M. Zoli, F. Forni, M.A. Vandelli, G. Tosi, A.M. Grabrucker, Application of Polymeric Nanoparticles for CNS Targeted Zinc Delivery In Vivo. CNS Neurol Disord Drug Targets 14(8) (2015) 1041-1053.

[20] A.M. Grabrucker, C.C. Garner, T.M. Boeckers, L. Bondioli, B. Ruozi, F. Forni, M.A. Vandelli, G. Tosi, Development of novel Zn2+ loaded nanoparticles designed for cell-type targeted drug release in CNS neurons: in vitro evidences. PLoS One 6(3) (2011) e17851.

[21] A.V. Vergoni, G. Tosi, R. Tacchi, M.A. Vandelli, A. Bertolini, L. Costantino, Nanoparticles as drug delivery agents specific for CNS: in vivo biodistribution. Nanomedicine 5(4) (2009) 369-377.

[22] L. Costantino, F. Gandolfi, G. Tosi, F. Rivasi, M.A. Vandelli, F. Forni, Peptidederivatized biodegradable nanoparticles able to cross the blood-brain barrier. J. Control. Release 108 (2005) 84-96.

[23] G. Tosi, B. Ruozi, D. Belletti, A. Vilella, M. Zoli, M.A. Vandelli, F. Forni, Brain-targeted polymeric nanoparticles: in vivo evidences after different routes of administration in rodents. Nanomedicine UK 8 (2013) 1373-1383.

[24] M.D. Blanco, M.J. Alonso, Development and characterization of protein-loaded poly(lactide-co-glycolide) nanospheres. Eur J Pharm Biopharm. 43 (1997) 287–294.

[25] A. Zanardi, R. Ferrari, G. Leo, U. Maskos, J.P. Changeux, M. Zoli, Loss of high-affinity nicotinic receptors increases the vulnerability to excitotoxic lesion and decreases the positive effects of an enriched environment. FASEB J 21(14) (2007) 4028-4037.

[26] A. Corradi, A. Zanardi, C. Giacomini, F. Onofri, F. Valtorta, M. Zoli, F. Benfenati, Synapsin-I- and synapsin-II-null mice display an increased age-dependent cognitive impairment. J Cell Sci 121(Pt 18) (2008) 3042-3051.

[27] P. Sapra, P. Tyagi, T.M. Allen, Ligand-targeted liposomes for cancer treatment. Curr Drug Deliv 2(4) (2005) 369-381.

[28] G. Tosi, L. Costantino, B. Ruozi, F. Forni, M.A. Vandelli, Polymeric nanoparticles for the drug delivery to the central nervous system. Expert Opin Drug Deliv 5(2) (2008) 155-174.

[29] K.D. Bornemann, M. Staufenbiel, Transgenic mouse models of Alzheimer's disease. Ann N Y Acad Sci 908 (2000) 260-266.

[30] J.A. Richardson, D.K. Burns, Mouse models of Alzheimer's disease: a quest for plaques and tangles. ILAR J 43(2) (2002) 89-99.

[31] R. Kayed, E. Head, F. Sarsoza, T. Saing, C.W. Cotman, M. Necula, L. Margol, J. Wu, L. Breydo, J.L. Thompson, S. Rasool, T. Gurlo, P. Butler, C.G. Glabe, Fibril specific,

conformation dependent antibodies recognize a generic epitope common to amyloid fibrils and fibrillar oligomers that is absent in prefibrillar oligomers. Mol Neurodegener 2 (2007) 18.

[32] D. Van Dam, R. D'Hooge, M. Staufenbiel, C. Van Ginneken, F. Van Meir, P.P. De Deyn, Age-dependent cognitive decline in the APP23 model precedes amyloid deposition. Eur J Neurosci 17(2) (2003) 388-396.

[33] H. Akiyama, S. Barger, S. Barnum, B. Bradt, J. Bauer, G.M. Cole, N.R. Cooper, P. Eikelenboom, M. Emmerling, B.L. Fiebich, C.E. Finch, S. Frautschy, W.S. Griffin, H. Hampel, M. Hull, G. Landreth, L. Lue, R. Mrak, I.R. Mackenzie, P.L. McGeer, M.K. O'Banion, J. Pachter, G. Pasinetti, C. Plata-Salaman, J. Rogers, R. Rydel, Y. Shen, W. Streit, R. Strohmeyer, I. Tooyoma, F.L. Van Muiswinkel, R. Veerhuis, D. Walker, S. Webster, B. Wegrzyniak, G. Wenk, T. Wyss-Coray, Inflammation and Alzheimer's disease. Neurobiol Aging 21(3) (2000) 383-421.

[34] E.M. Sutinen, T. Pirttilä, G. Anderson, A. Salminen, J.O. Ojala, Pro-inflammatory interleukin-18 increases Alzheimer's disease-associated amyloid-β production in human neuron-like cells. J Neuroinflammation 9 (2012) 199.

[35] J. Ojala, I. Alafuzoff, S.K. Herukka, T. van Groen, H. Tanila, T. Pirttilä, Expression of interleukin-18 is increased in the brains of Alzheimer's disease patients. Neurobiol Aging 30(2) (2009) 198-209.

[36] R.T. Perry, J.S. Collins, H. Wiener, R. Acton, R.C. Go, The role of TNF and its receptors in Alzheimer's disease. Neurobiol Aging 22(6) (2001) 873-883.

[37] E. Masliah, M. Mallory, M. Alford, R. DeTeresa, L.A. Hansen, D.W. McKeel, J.C. Morris, Altered expression of synaptic proteins occurs early during progression of Alzheimer's disease. Neurology 56(1) (2001) 127-129.

[38] C.A. Davies, D.M. Mann, P.Q. Sumpter, P.O. Yates, A quantitative morphometric analysis of the neuronal and synaptic content of the frontal and temporal cortex in patients with Alzheimer's disease. J Neurol Sci 78(2) (1987) 151-164.

[39] P.H. Reddy, G. Mani, B.S. Park, J. Jacques, G. Murdoch, W. Whetsell, J. Kaye, M. Manczak, Differential loss of synaptic proteins in Alzheimer's disease: implications for synaptic dysfunction. J Alzheimers Dis 7(2) (2005) 103-117; discussion 173-180.

[40] A. Rijal Upadhaya, F. Scheibe, I. Kosterin, D. Abramowski, J. Gerth, S. Kumar, S. Liebau, H. Yamaguchi, J. Walter, M. Staufenbiel, D.R. Thal, The type of Aβ-related neuronal degeneration differs between amyloid precursor protein (APP23) and amyloid β-peptide (APP48) transgenic mice. Acta Neuropathol Commun 1 (2013) 77.

[41] C.J. Frederickson, J.Y. Koh, A.I. Bush, The neurobiology of zinc in health and disease. Nat Rev Neurosci 6(6) (2005) 449-462.

[42] A.M. Grabrucker, M.J. Knight, C. Proepper, J. Bockmann, M. Joubert, M. Rowan, G.U. Nienhaus, C.C. Garner, J.U. Bowie, M.R. Kreutz, E.D. Gundelfinger, T.M. Boeckers, Concerted action of zinc and ProSAP/Shank in synaptogenesis and synapse maturation. EMBO J 30(3) (2011) 569-581.

[43] A.M. Grabrucker, A role for synaptic zinc in ProSAP/Shank PSD scaffold malformation in autism spectrum disorders. Dev Neurobiol 74(2) (2014) 136-146.

[44] C. Corona, F. Masciopinto, E. Silvestri, A.D. Viscovo, R. Lattanzio, R.L. Sorda, D. Ciavardelli, F. Goglia, M. Piantelli, L.M. Canzoniero, S.L. Sensi, Dietary zinc supplementation of 3xTg-AD mice increases BDNF levels and prevents cognitive deficits as well as mitochondrial dysfunction. Cell Death Dis 1:e91 (2010).

[45] S.D. Kuipers, C.R. Bramham, Brain-derived neurotrophic factor mechanisms and function in adult synaptic plasticity: new insights and implications for therapy. Curr Opin Drug Discov Devel 9(5) (2006) 580-586.

[46] S.X. Bamji, B. Rico, N. Kimes, L.F. Reichardt, BDNF mobilizes synaptic vesicles and enhances synapse formation by disrupting cadherin-beta-catenin interactions. J Cell Biol 174(2) (2006) 289-299.

[47] D.J. Eide, The oxidative stress of zinc deficiency. Metallomics 3(11) (2011) 1124-1129.

[48] J.L. Cummings,The Neuropsychiatric Inventory: assessing psychopathology in dementia patients. Neurology 48(5 Suppl 6) (1997) 10-16.

[49] F.J. Gil-Bea, B. Aisa, R. Schliebs, M.J. Ramírez, Increase of locomotor activity underlying the behavioral disinhibition in tg2576 mice. Behav Neurosci 121(2) (2007) 340-344.

[50] R.G. Phillips, J.E. LeDoux, Differential contribution of amygdala and hippocampus to cued and contextual fear conditioning. Behav Neurosci 106(2) (1992) 274-285.

[51] R.A. Cherny, C.S. Atwood, M.E. Xilinas, D.N. Gray, W.D. Jones, C.A. McLean, K.J. Barnham, I. Volitakis, F.W. Fraser, Y. Kim, X. Huang, L.E. Goldstein, R.D. Moir, J.T. Lim, K. Beyreuther, H. Zheng, R.E. Tanzi, C.L. Masters, A.I. Bush, Treatment with a copper-zinc chelator markedly and rapidly inhibits beta-amyloid accumulation in Alzheimer's disease transgenic mice. Neuron 30(3) (2001) 665-676.

[52] T. Wang, C.Y. Wang, Z.Y. Shan, W.P. Teng, Z.Y. Wang, Clioquinol reduces zinc accumulation in neuritic plaques and inhibits the amyloidogenic pathway in AβPP/PS1 transgenic mouse brain. J Alzheimers Dis 29(3) (2012) 549-559.

[53] E.J. Lee, H. Lee, T.N. Huang, C. Chung, W. Shin, K. Kim, J.Y. Koh, Y.P. Hsueh, E. Kim, Trans-synaptic zinc mobilization improves social interaction in two mouse models of autism through NMDAR activation. Nat Commun 6:7168 (2015).

[54] A.R. White, T. Du, K.M. Laughton, I. Volitakis, R.A. Sharples, M.E. Xilinas, D.E. Hoke, R.M. Holsinger, G. Evin, R.A. Cherny, A.F. Hill, K.J. Barnham, Q.X. Li, A.I. Bush, C.L. Masters, Degradation of the Alzheimer disease amyloid beta-peptide by metal-dependent up-regulation of metalloprotease activity. J Biol Chem 281(26) (2006) 17670-17680.

Figure Legends

Figure 1: Characteriztion of Nanoparticles. A) Chemico-physical and technological parameters of samples. Z-Average, PDI (polidispersivity index) and Z-pot (Zeta Potential) of NPs in distilled water after the purification process. The percentage of encapsulation efficiency (EE) was determined as the ratio of the encapsulated out of the total (encapsulated + free) drug per cent (%). The percentage of loading capacity (LC) was expressed as the ratio of the encapsulated drug out of the total mass (encapsulated drug + polymer) per cent. For both EE and LC, values refer to the content of Zn^{2+} considering that 1 mg of $ZnSO_4$ contains 0.40 mg of Zn^{2+}.The percentage of yield was expressed as the ratio of the recovered freeze-dried sample (excluding residual PVA) out of the total mass weighted (polymer and drug) per cent. B) SEM analyses of g7-NPs and g7-NP-Zn. C) The profile for Zn^{2+} diffusion and the release from g7-NP-Zn was measured in distilled water and phosphate buffer pH 7.4. Zn^{2+} rapidly diffused (within 60 min) from the dialyses membrane independently from the medium (water of phosphate buffer, C1). The release profile of Zn^{2+} from g7-NP-Zn in water showed an initial "burst release" (about 20%) during the first 5 min, followed by an intermediate slow release phase (5-50 min) and a second burst release. Total Zn^{2+} release was detected in water over 120 min. The same experiment performed using phosphate buffer (higher ionic strength) showed a faster and more linear release of Zn^{2+} which was completed within 110 min (C2).

Figure 2: Reduced plaque size in animals treated with zinc-loaded nanoparticles. Brain sections from WT and APP23 mice were obtained after treatments and plaques were visualized using anti- Aβ antibodies staining. A) The mean area of plaques in cortex was measured from at least three optic fields of three sections per mouse. Exemplary images are shown in (B). Additionally, DAPI staining is shown visualizing cell nuclei. A significant reduction in mean plaque area compared to saline treated controls can be seen after treatment with g7-NPs-Zn in APP23 mice (one-way ANOVA, $F = 7.549$, $p = 0.012$; Post test shows a significant difference between $APP23_{saline}$ and $APP23_{g7\text{-}NPs\text{-}Zn}$ $p = 0.0044$, and $APP23_{g7\text{-}NPs}$ and $APP23_{g7\text{-}NPs\text{-}Zn}$ $p = 0.0294$). No plaques were detected in WT animals. C) The mean number of plaques per area was not significantly altered by the treatments. (n = 7 mice: WT_{saline}, $APP23_{saline}$, $WT_{g7\text{-}NPs}$; n = 6: $APP23_{g7\text{-}NPs}$; n = 18: $WT_{g7\text{-}NPs\text{-}Zn}$, $APP23_{g7\text{-}NPs\text{-}Zn}$). D) Brain sections from APP23 mice were obtained after treatments and plaques were visualized using Thioflavin. The mean area and the number of plaques in cortex was measured. A significant difference was detected for the parameter plaque area (one-way ANOVA, $F = 4.656$, $p = 0.032$). Post hoc analysis shows a significant difference in plaque area in mice treated with g7-NPs-Zn compared to saline ($p = 0.0443$) and empty g7-NPs ($p = 0.0297$). No significant differences were observed regarding the number of plaques (one-way ANOVA, $F = 2.4$, $p = 0.133$) (n = 5 mice ($APP23_{saline}$), n = 4 mice ($APP23_{g7\text{-}NPs}$), n = 6 mice ($APP23_{g7\text{-}NPs\text{-}Zn}$)). E) Exemplary images using Thioflavin (green) showslightly less plaques with less area in APP23 mice treated with g7-NPs-Zn. F) Dot Blot analysis using the OC antibody. Left: Exemplary signals. WT mice show only background signals. A reduction of OC immunoreactive signals is seen in APP23 mice injected with g7-NP-Zn as a trend (one-way ANOVA, $F = 3.662$, $p = 0.091$).

Figure 3: Reduced plaque size in animals treated with zinc-loaded nanoparticles detected by zinc-staining. A) The mean area of plaques in cortex was measured from at least three optic fields of three sections per mouse. Exemplary images are shown. Additionally, DAPI staining is shown visualizing cell nuclei. B) A significant reduction in mean plaque area compared to saline treated controls can be seen after treatment with g7-NPs-Zn in APP23 mice (ANOVA on ranks, $H = 55.676$, $p < 0.001$; Post test shows a significant difference

between $APP23_{saline}$ and $APP23_{g7\text{-}NPs\text{-}Zn}$ $p = 0.032$). No plaques were detected in WT animals. C) The mean number of plaques per area was not significantly altered by the treatments (n = 7 mice: WT_{saline}, $APP23_{saline}$, $WT_{g7\text{-}NPs}$; n = 6: $APP23_{g7\text{-}NPs}$; n = 18: $WT_{g7\text{-}NPs\text{-}Zn}$, $APP23_{g7\text{-}NPs\text{-}Zn}$).

Figure 4: Altered inflammatory markers in animals treated with zinc-loaded nanoparticles. Zinc levels of individuals correlate with levels of IL-6 and IL-18 in APP23 mice. Inflammatory markers were measured in brain tissue of each mouse using qRT-PCR approaches. Virtual mRNA expression levels were calculated and are shown normalized against HMBS. For each animal, technical triplicates were performed. A) APP23 mice show increased levels of IL-6 (ANOVA on ranks, H = 11.428, $p = 0.0435$; Dunn's post test: WT_{saline} vs $APP23_{saline}$ $p = 0.1775$, and $WT_{g7\text{-}NP}$ vs $APP23_{g7\text{-}NP}$ $p = 0.0043$). Post hoc analysis shows a significant reduction in IL-6 levels after treatment with g7-NPs-Zn in APP23 mice compared to $APP23_{g7\text{-}NP}$ $p = 0.0275$, but not compared to $APP23_{saline}$ $p = 0.0754$. The treatment did not affect WT animals. B) APP23 mice show slightly different levels of IL-18 (ANOVA on ranks, H = 15.188, $p = 0.0096$). Post hoc analysis shows a significant reduction in IL-18 levels after treatment with g7-NPs-Zn in APP23 mice compared to $APP23_{saline}$ $p = 0.0094$, and $APP23_{g7\text{-}NP}$ $p = 0.0245$. The treatment did not affect WT animals despite a reduction in IL-18 levels seen in $WT_{g7\text{-}NP}$ compared to WT_{Saline}. C) APP23 mice show increased levels of TNF-1. However, none of the groups and treatment conditions reveal significant alterations (ANOVA on ranks, H = 6.058, $p = 0.3006$). D) APP23 mice show increased levels of IL-10 (WT_{saline} vs. APP_{saline} $p = 0.4206$; $WT_{g7\text{-}NP}$ vs. $APP_{g7\text{-}NP}$ $p = 0.0152$, U-test). Upon treatment with g7-NPs-Zn, IL-10 levels are significantly increased in both WT (WT_{saline} vs $WT_{g7\text{-}NPs\text{-}Zn}$ $p = 0.0074$, U-test) and not significantly in APP23 (APP_{saline} vs $APP_{g7\text{-}NPs\text{-}Zn}$ $p = 0.55$, U-test) mice. E,F) Brain-zinc concentrations of each mouse were measured by AAS and plotted against the expression levels of IL-6 (E) and IL-18 (F) of the same individual. A significant correlation between brain-zinc levels and the detected expression of IL-6 and IL-18 can be observed in APP23 but not WT mice (large panels) (Linear Regression analysis: APP23 $p < 0.001$). With increasing zinc levels, the expression of the pro-inflammatory cytokines decreases. Small inserts: The correlation is found significant in the groups treated with g7-NP and g7-NP-Zn for IL-6, and g7-NP-Zn for IL-18.

Figure 5: Unaltered synapse density in APP23 animals treated with zinc-loaded nanoparticles compared to WT mice. Zinc levels of individuals correlate with synapse density in APP23 mice. Brain sections from WT and APP23 mice were obtained after treatments and synapses labeled with anti-Bassoon staining. A) The mean number of immunoreactive signals per area (33,750 $pixel^2$) in cortex was measured from at least three optic fields of three sections per mouse. Exemplary images are shown in (B). The results show no significant differences (one-way ANOVA, F = 0.3785, $p = 0.8614$). However, a not significant difference in the number of Bassoon signals in APP23 mice compared to WT under control conditions is visible (n.s. = not significant; p = 0.14). In APP23 mice treated with g7-NPs-Zn, no reduction in synapse density is detected compared to WT mice. C) Brain-zinc concentrations of each mouse were measured by AAS and plotted against the number of synapses per area of the same individual. Large panels: Combining all animals from each treatment group, a significant correlation between zinc levels and synapse density can be observed in APP23 mice but not WT mice (Linear Regression analysis: APP23 r = 0.677, $p < 0.001$; WT r = 0.206, p = 0.249). Small inserts: The correlation is present in APP23 mice within each treatment group.

Figure 6: Reduced hyperlocomotion in APP23 mice treated with g7-NP-Zn. A-B) Locomotion in an open field. Total number of transitions and entries into the center zone are

shown. Two-way ANOVA showed a significant genotype effect for both total entries ($F_{1,57}$ = 13.02, p < 0.001, panel A) and entries from border to center zone ($F_{1,57}$ = 15.56, p < 0.001, panel B). Post-hoc comparisons using unpaired *t*-test, * = p < 0.05. C) Elevated plus maze. The number of entries into the open arms per total entries (entries in closed = entries in open arm) are shown. Two way ANOVA showed no significant genotype or treatment effect ($F_{2,44}$ = 0.463, p = 0.632). D) Contextual fear conditioning. Percent freezing time is shown. Two way ANOVA showed no significant genotype or treatment effect ($F_{1,57}$ = 1.21, p = 0.276).

Figure S1: A) Brain lysate from WT and APP23 mice was obtained after behavioral experiments and zinc levels measured by AAS. The mean levels per group are shown. No significant differences were seen between the groups (one-way ANOVA, F = 0.465, *p* = 0.801). B) Brain sections from APP23 mice were obtained after treatments and plaques were visualized using Thioflavin. The mean area and the number of plaques in the hippocampus was measured. No significant difference was detected for the parameter plaque area (one-way ANOVA, F = 0.585, *p* = 0.575). No significant differences were observed regarding the number of plaques (one-way ANOVA, F = 0.425, *p* = 0.665) (n = 5 mice ($APP23_{saline}$), n = 4 mice ($APP23_{g7\text{-}NPs}$), n = 4 mice ($APP23_{g7\text{-}NPs\text{-}Zn}$)).

Figure 1

A

	Chemico-physical parameters					Technological Characterization		
Sample	**Z-Average (nm) [± SD]**	**PDI [± SD]**	**Di50 (nm) [± SD]**	**Di90 (nm) [± SD]**	**Z-pot (mV) [± SD]**	**LC (%) [± SD]**	**EE (%) [± SD]**	**yield (%) [± SD]**
g7-NP	203 [±14]	0.08 [±0.04]	208 [±15]	308 [±39]	-22.3 [±7.1]	-	-	89 [±3]
g7-NP-Zn	220 [±15]	0.15 [±0.05]	224 [±13]	348 [±60]	-4.2 [±0.5]	7.2 [±1.1]	5 [±1]	85 [±2]

B

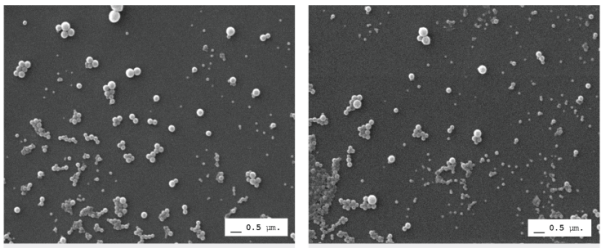

g7-NP **g7-NP-Zn**

C

C1

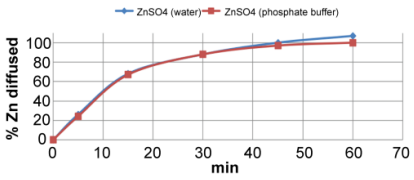

C2

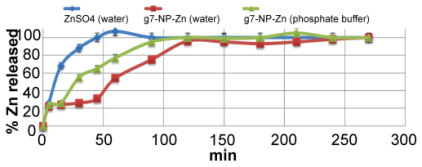

Figure 2

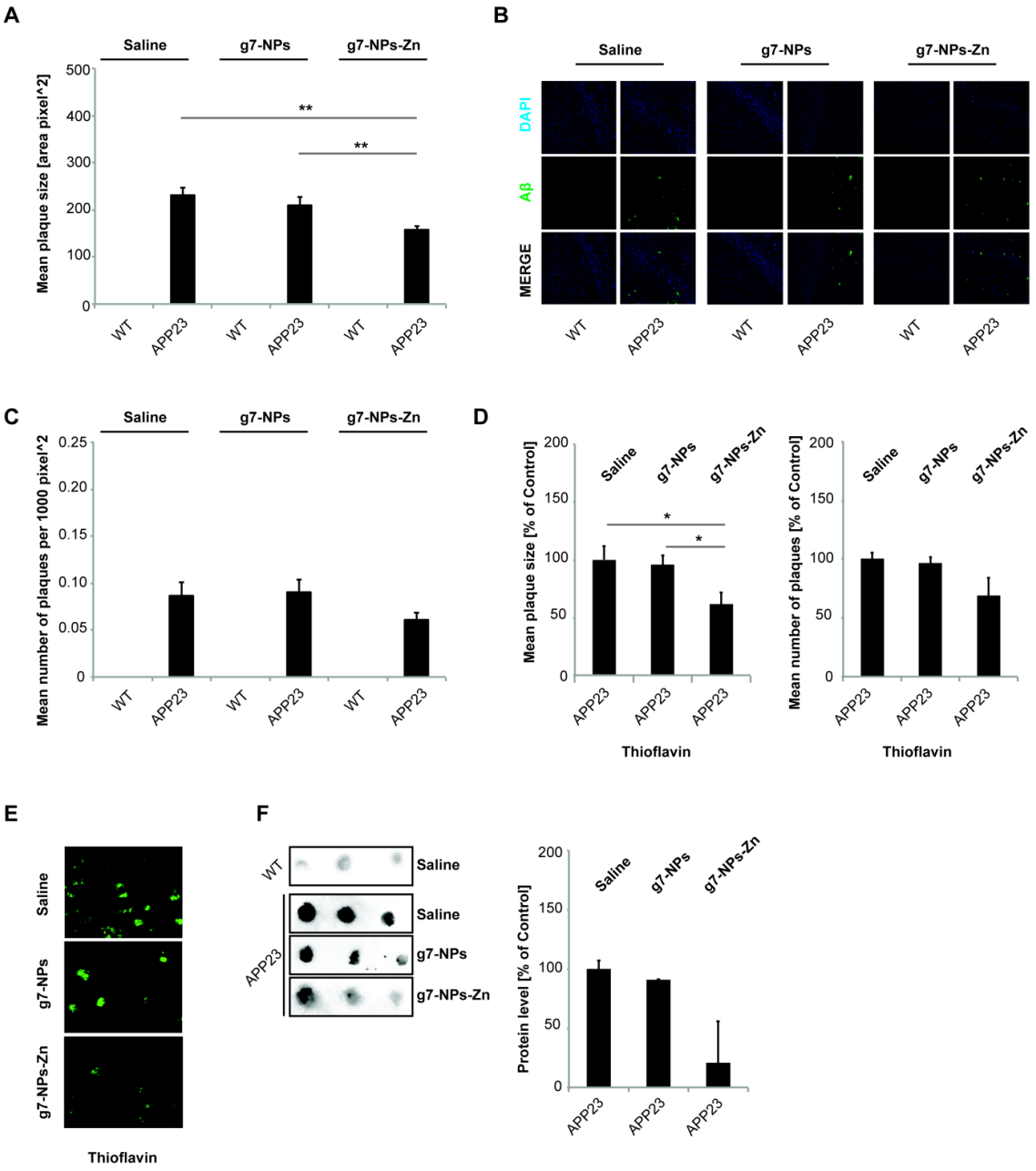
A
Saline
g7-NPs
g7-NPs-Zn
Mean plaque size [area pixel^2]
500
400
300
200
100
0
**
**
WT
APP23
WT
APP23
WT
APP23
B
Saline
g7-NPs
g7-NPs-Zn
DAPI
Aβ
MERGE
WT
APP23
WT
APP23
WT
APP23
C
Saline
g7-NPs
g7-NPs-Zn
Mean number of plaques per 1000 pixel^2
0.25
0.20
0.15
0.10
0.05
0
WT
APP23
WT
APP23
WT
APP23
D
Saline
g7-NPs
g7-NPs-Zn
Mean plaque size [% of Control]
200
150
100
50
0
*
*
APP23
APP23
APP23
Thioflavin
Saline
g7-NPs
g7-NPs-Zn
Mean number of plaques [% of Control]
200
150
100
50
0
APP23
APP23
APP23
Thioflavin
E
Saline
g7-NPs
g7-NPs-Zn
Thioflavin
F
WT
Saline
APP23
Saline
g7-NPs
g7-NPs-Zn
Saline
g7-NPs
g7-NPs-Zn
Protein level [% of Control]
200
150
100
50
0
APP23
APP23
APP23

Figure 3

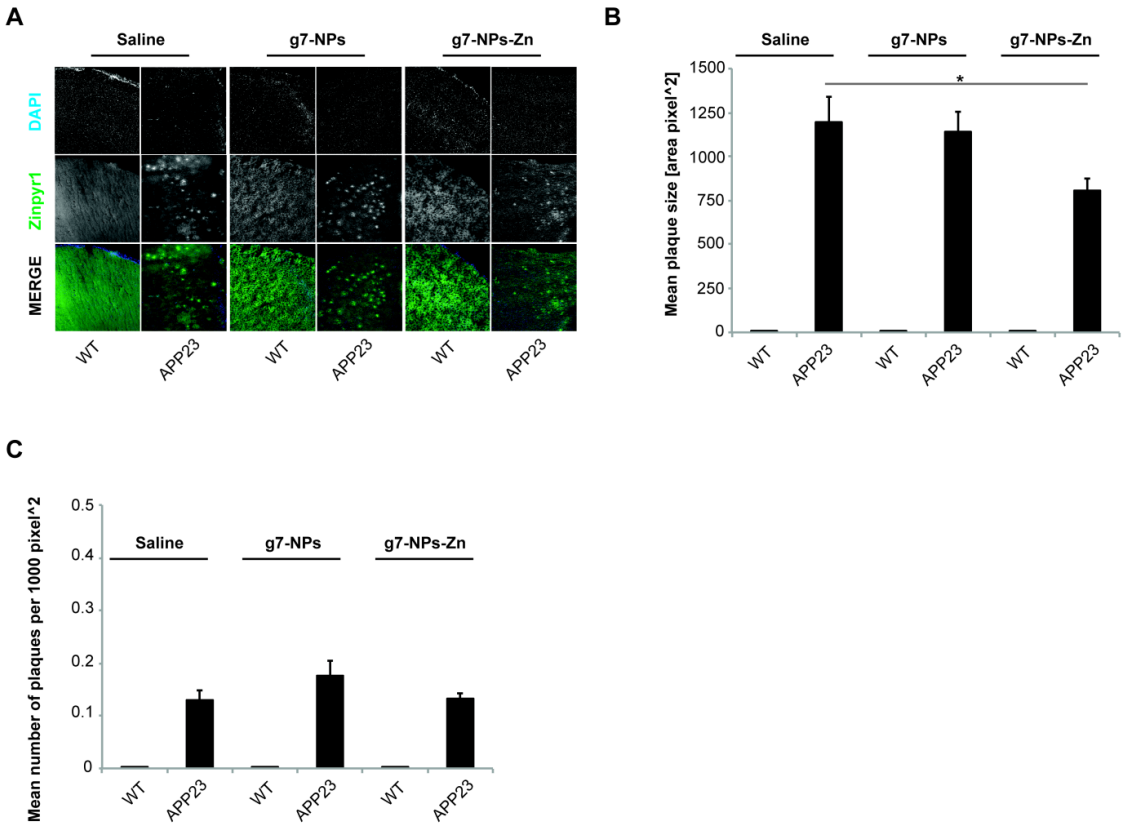
A
Saline
g7-NPs
g7-NPs-Zn
DAPI
Zinpyr1
MERGE
WT
APP23
B
Mean plaque size [area pixel^2]
1500
1250
1000
750
500
250
0
*
C
Mean number of plaques per 1000 pixel^2
0.5
0.4
0.3
0.2
0.1
0

Figure 4

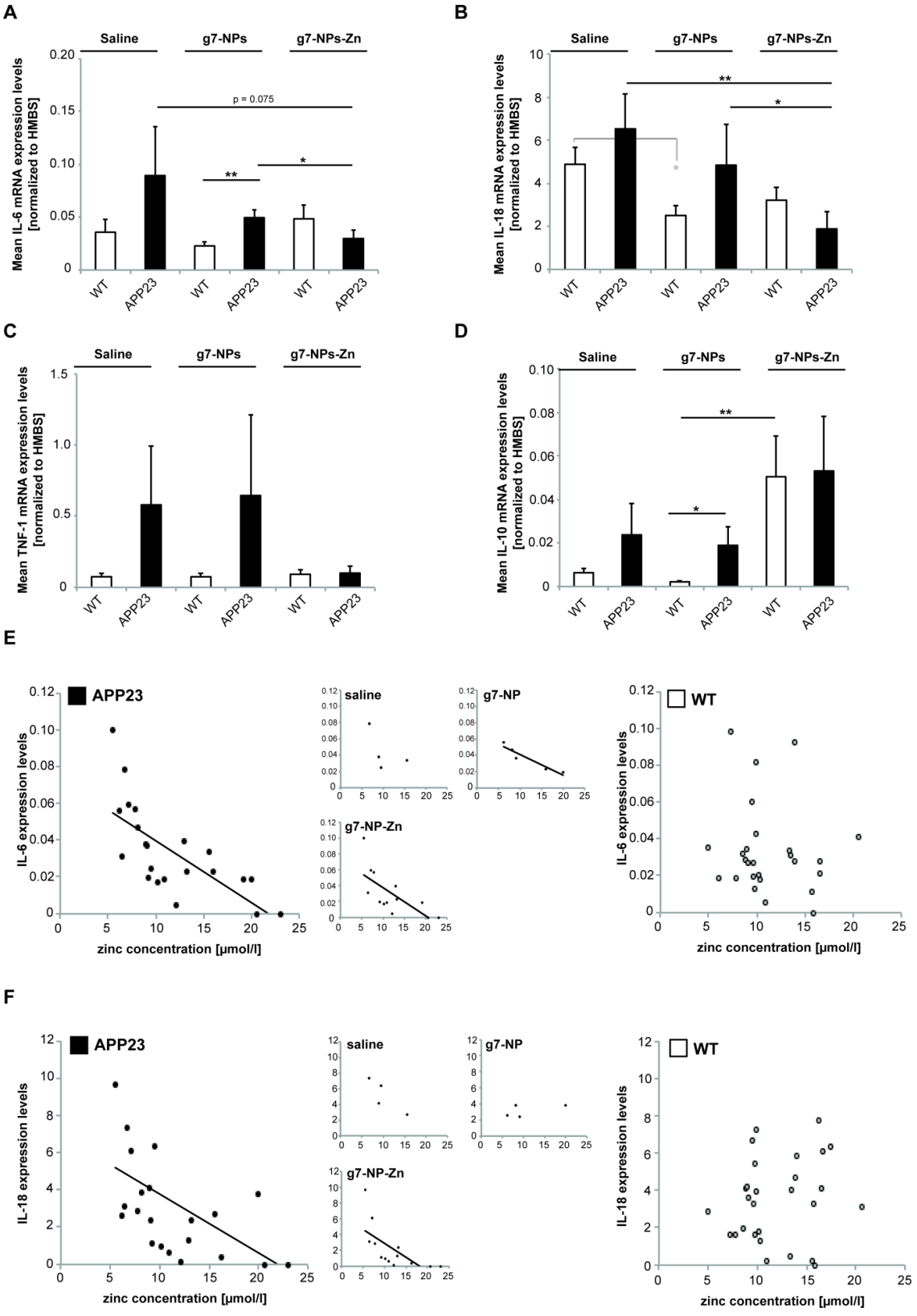
A
Saline
g7-NPs
g7-NPs-Zn
Mean IL-6 mRNA expression levels [normalized to HMBS]
p = 0.075
**
*
WT
APP23
B
Mean IL-18 mRNA expression levels [normalized to HMBS]
C
Mean TNF-1 mRNA expression levels [normalized to HMBS]
D
Mean IL-10 mRNA expression levels [normalized to HMBS]
E
APP23
saline
g7-NP
g7-NP-Zn
WT
IL-6 expression levels
zinc concentration [µmol/l]
F
IL-18 expression levels

Figure 5

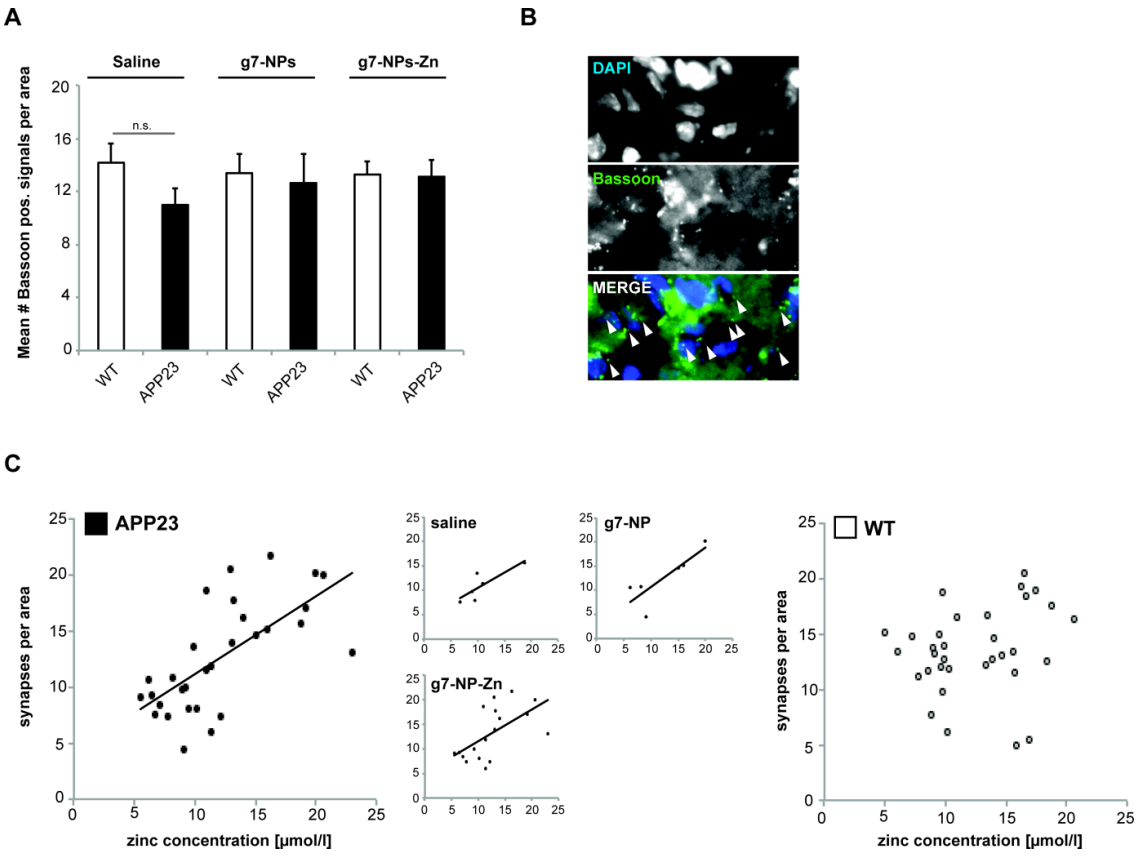
A
Saline
g7-NPs
g7-NPs-Zn
n.s.
Mean # Bassoon pos. signals per area
WT
APP23
B
DAPI
Bassoon
MERGE
C
APP23
saline
g7-NP
g7-NP-Zn
WT
synapses per area
zinc concentration [µmol/l]

Figure 6

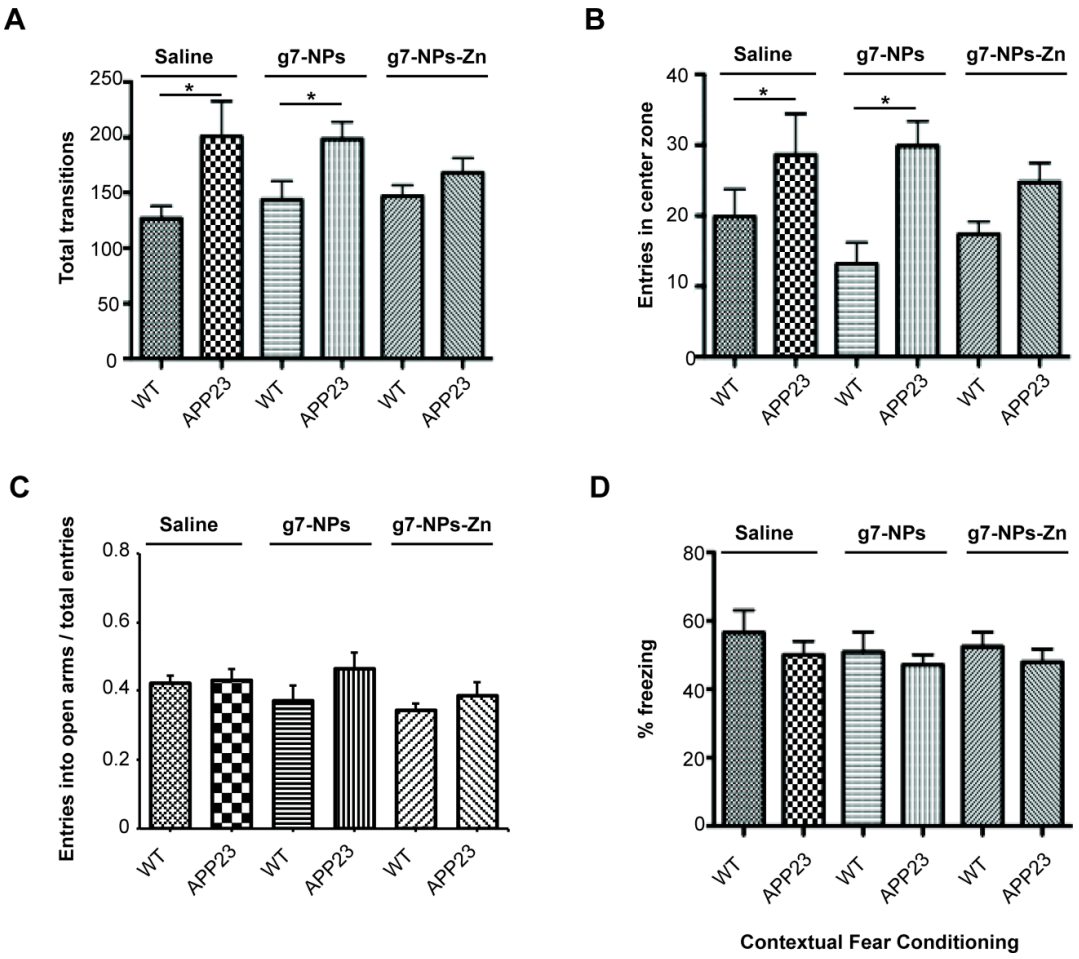
A
Saline
g7-NPs
g7-NPs-Zn
Total transitions
250
200
150
100
50
0
*
*
WT
APP23
WT
APP23
WT
APP23
B
Saline
g7-NPs
g7-NPs-Zn
Entries in center zone
40
30
20
10
0
*
*
WT
APP23
WT
APP23
WT
APP23
C
Saline
g7-NPs
g7-NPs-Zn
Entries into open arms / total entries
0.8
0.6
0.4
0.2
0
WT
APP23
WT
APP23
WT
APP23
D
Saline
g7-NPs
g7-NPs-Zn
% freezing
80
60
40
20
0
WT
APP23
WT
APP23
WT
APP23
Contextual Fear Conditioning

Figure S1

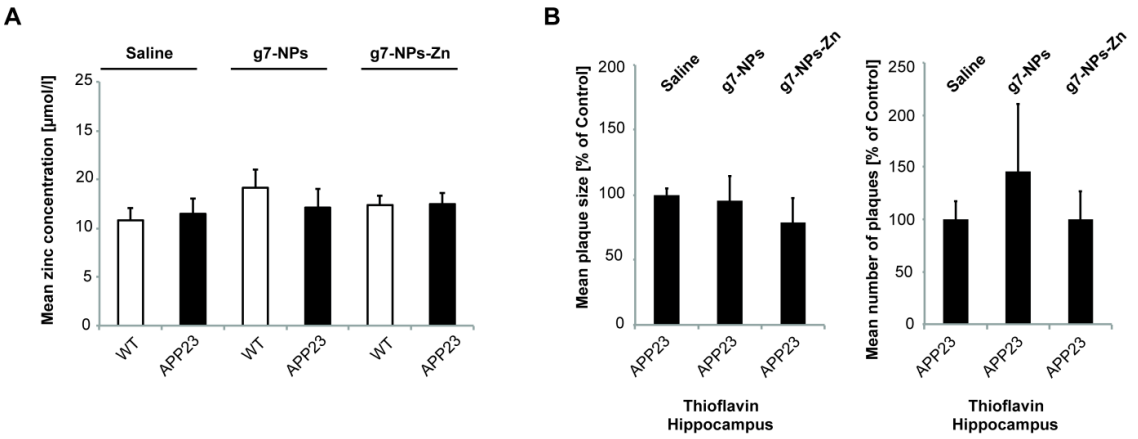
A
Saline
g7-NPs
g7-NPs-Zn
Mean zinc concentration [µmol/l]
25
15
20
10
5
0
WT
APP23
WT
APP23
WT
APP23
B
Mean plaque size [% of Control]
200
150
100
50
0
Saline
g7-NPs
g7-NPs-Zn
APP23
APP23
APP23
Thioflavin
Hippocampus
Mean number of plaques [% of Control]
250
200
150
100
50
0
Saline
g7-NPs
g7-NPs-Zn
APP23
APP23
APP23
Thioflavin
Hippocampus